AMERICAN SOCIETY FOR MICROBIOLOGY | Molecular and Cellular Biology®

RESEARCH ARTICLE

DNA Damage-Induced Phosphorylation of Histone H2A at Serine 15 Is Linked to DNA End Resection

Salar Ahmad,[a] Valérie Côté,[a] Jacques Côté[a]

[a]St-Patrick Research Group in Basic Oncology, Centre Hospitalier Universitaire de Québec-Université Laval Research Center, Laval University Cancer Research Center, Quebec City, Quebec, Canada

ABSTRACT The repair of DNA double-strand breaks (DSBs) occurs in chromatin, and several histone posttranslational modifications have been implicated in the process. Modifications of the histone H2A N-terminal tail have also been linked to DNA damage response, through acetylation or ubiquitination of lysine residues that regulate repair pathway choice. Here, we characterize a new DNA damage-induced phosphorylation on chromatin, at serine 15 of H2A in yeast. We show that this SQ motif functions independently of the classical S129 C-terminal site (γ-H2A) and that mutant-mimicking constitutive phosphorylation increases cell sensitivity to DNA damage. H2AS129ph is induced by Tel1^{ATM} and Mec1^{ATR}, and the loss of Lcd1^{ATRIP} or Mec1 signaling decreases γ-H2A spreading distal to the DSB. In contrast, H2AS15ph is completely dependent on Lcd1^{ATRIP}, indicating that this modification only happens when end resection is engaged. This is supported by an increase in replication protein A (RPA) and a decrease in DNA signal near the DSB in *H2A-S15E* phosphomimic mutants, indicating higher resection. In mammals, this serine is replaced by a lysine (H2AK15) which undergoes an acetyl-monoubiquityl switch to regulate binding of 53BP1 and resection. This regulation seems functionally conserved with budding yeast H2AS15 and 53BP1-homolog Rad9, using different posttranslational modifications between organisms but achieving the same function.

KEYWORDS DNA damage, double strand break, H2A, Rad9, histone phosphorylation, resection

The genetic information of the cell is challenged by various endogenous and exogenous cues which lead to DNA damage. If unchecked, this can lead to mutations, translocations, and loss of genetic information, and in higher eukaryotes, it can be the underlying cause for diseases such as cancer (1, 2). One of the most harmful forms of DNA damage is a DNA double-strand break (DSB). To endure and mitigate such damage to the DNA, cells orchestrate cell cycle arrest and DNA repair pathways, collectively termed the DNA damage response (DDR). The two main pathways for DSB repair are nonhomologous end joining (NHEJ) and homologous recombination (HR). NHEJ involves direct ligation of the two broken DNA ends, which may require some processing, making it a more error-prone pathway (3). In HR, single-stranded DNA (ssDNA) is generated through a process called resection, which involves the use of a homologous sequence or sister chromatid as a template to copy the genetic information, ensuring a lower error rate (4).

The phosphatidylinositol-3-OH kinase-related kinases (PIKKs) family plays an important role in DDR. It includes *Saccharomyces cerevisiae* Tel1 and Mec1, and mammalian ataxia telangiectasia-mutated (ATM), AT-related (ATR), and DNA-dependent protein kinase (DNA-PK) (5, 6). One of the first DNA damage-dependent chromatin modifications to be identified was γ-H2A (X), which is the phosphorylation of histone H2A at S129 in yeast and histone H2AX at S139 in mammals (7–9). This phosphorylation is carried out by both Tel1/ATM and Mec1/ATR. In yeast, H2AS129ph spreads to more than 50 kb on both sides flanking the DSB, whereas in mammals it covers up to a megabase (10, 11). This histone mark is implicated in the DNA damage

Citation Ahmad S, Côté V, Côté J. 2021. DNA damage-induced phosphorylation of histone H2A at serine 15 is linked to DNA end resection. Mol Cell Biol 41:e00056-21. https://doi.org/10.1128/MCB.00056-21.

Address correspondence to Jacques Côté, jacques.cote@crhdq.ulaval.ca.

Received 7 February 2021
Returned for modification 19 March 2021
Accepted 21 September 2021
Accepted manuscript posted online 27 September 2021
Published 22 November 2021

response and is required for proper recruitment of several repair/signaling factors as well as chromatin remodelers/modifiers (12–17). H2AX$^{-/-}$ mice are radiation sensitive, growth retarded, and immune deficient, showing recruitment defects for a variety of repair factors such as Nbs1, 53BP1, and BRCA1 (18).

Interestingly, budding yeast has another Tel1/Mec1-dependent SQ phosphorylation site at the H2B C terminus, H2BT129ph, which largely correlates with H2AS129ph but is modulated by it (10). Other DNA damage-induced phosphorylation marks have been mapped on chromatin but are not deposited by PIKKs. In yeast, these include H4S1ph, H2AS122ph, and H2AT126ph, which have been linked to processes such as chromatin restoration after repair, meiosis, HR, and repair of fragile sites with CAG/CTG repeats (19–23). Apart from phosphorylation, other histone modifications such as acetylation, methylation, ubiquitylation, and SUMOylation have been implicated in DDR (16). In mammals, H2AK15 is ubiquitinated by RNF168, and this mark is responsible for recruitment and repair foci formation of 53BP1 in combination with H4K20me2, inhibiting resection and favoring NHEJ (24). At DSBs, the TIP60 complex can acetylate H2AK15 and bind H4K20me, thus antagonizing 53BP1 and favoring repair by HR (25). In budding yeast, Rad9 is the functional homolog of 53BP1, containing a Tudor domain which binds H3K79me (equivalent to mammalian H4K20) and a BRCT domain which recognizes γ-H2A (17, 26, 27). Both domains are required for the recruitment and retention of Rad9 at DSBs (17, 28). In contrast to 53BP1, Rad9 does not have a ubiquitin-binding domain, and yeast H2A does not have lysine corresponding to human H2AK15 (Fig. 1A). Instead, yeast H2A has a SQ site at this position which has been found to be phosphorylated in a Mec1-dependent manner upon DNA damage, in a large phosphoproteomic study (29).

This led us to investigate whether H2AS15 has a role in the repair of DNA breaks. Our results indicate that H2AS15ph is induced by Mec1^{ATR} over a large domain of chromatin around the DSB. Our data also suggest that H2AS15ph regulates Rad9 binding and DNA end resection. Altogether, these results suggest an evolutionary conserved mechanism, similar to the mammalian H2AK15 ubiquitin/acetylation switch, which modulates yeast Rad9^{53BP1} function on the chromatin surrounding DNA breaks.

RESULTS

H2AS15ph function is distinct from H2AS129ph in response to DNA damage. In order to investigate whether H2A-S15 has a role in DNA damage response, we mutated H2A-S15 to alanine (non-phosphorylation mimicking) or glutamic acid (phosphorylation mimicking). In the presence of the DNA-damaging agent methyl methanesulfonate (MMS), *H2A-S15E* mutant cells show a slight growth defect, which is not seen for *H2A-S15A* (Fig. 1B). However, in combination with the *H2A-S129A* mutant, both *H2A-S15A/E* show stronger growth defects compared to single *H2A-S129A* mutant cells (Fig. 1B). Next, we tested whether the *H2A-S15* mutants had any genetic interaction with H2BT129ph, the other PIKK-dependent histone phosphorylation induced in response to DSBs in yeast (10). *H2A-S15A/E H2B-T129A* double mutant cells do not show any additional growth defects compared to *H2A-S15* single mutants in the presence of MMS (Fig. 1C). These results indicate that H2AS129 and H2AS15 phosphorylations play distinct roles in response to DNA damage induced by MMS.

To determine whether the *H2A-S15* mutants affect H2AS129 phosphorylation *in vivo*, we performed ChIP-qPCR at an inducible DSB. We used the yeast background in which a single persistent DNA double strand break is created at the *MAT* locus by the homothallic endonuclease (HO), inducible by galactose-containing medium. The induced H2AS129ph signal detected on each side of the DSB in wild type (WT) cells corresponds to what was previously reported (10, 12). Both *H2A-S15A/E* mutants show a similar pattern of H2AS129ph compared to WT cells, not affecting the induction or spreading of H2A-S129ph besides a very small increase in the *H2A-S15E* mutant (Fig. 1D and E). These results again suggest that H2AS15ph has a role in DNA damage response/repair that is distinct from H2AS129ph.

The lysine residues of the H2A and H4 N-terminal tails are known targets of the NuA4 acetyltransferase complex (30). Studies have described histone modifications which modulate the

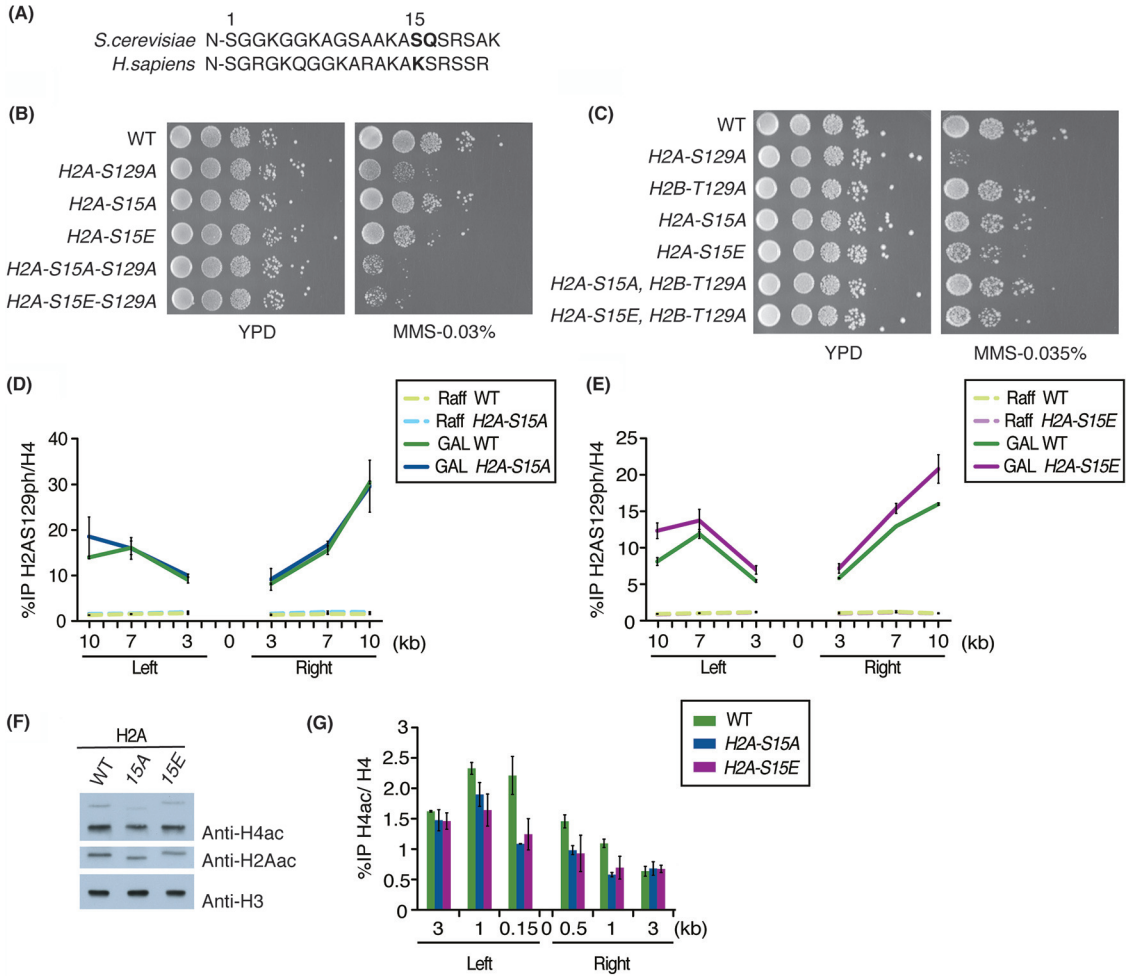

FIG 1 *H2A-S15* mutants are sensitive to DNA damage and function independently of γ-H2A. (A) Sequence of H2A N termini highlighting the SQ site at position 15 in *S. cerevisiae* and the corresponding lysine at position 15 in *H. sapiens*. (B and C) Phenotypic analysis of yeast cells expressing wild type or the indicated H2A mutants. Tenfold serial dilutions of log phase cells were spotted on plates containing rich medium either alone or in the presence of DNA-damaging agent methylmethane sulfonate (MMS). *H2A-S15E* showed a slight growth defect in the presence of the drug, whereas both *H2A-S15A/E* in background with *H2A-S129A* showed stronger sensitivity than their respective single mutants. *H2B-T129A* did not influence the growth of *H2A-S15A/E*. (D and E) ChIP-qPCR showing that γ-H2A at an inducible DSB is not affected by *H2A-S15A/E*. Cells were grown in YP-raffinose overnight until the log phase, followed by addition of galactose to induce DSB for 3 h before cross-linking the chromatin. Primer pairs used flanked the DNA sequence on both the left and right sides at 3 kb, 7 kb, and 10 kb of the DSB at *MAT* locus. Anti-H4 signal was used to normalize for histone occupancy. Data represents the mean of two independent biological replicates. Error bars indicate the range between the two biological replicates. (F) *H2A-S15A/E* affects the acetylation of histone H4 and H2A. Western blotting analysis of yeast whole-cell extracts (WCE) with anti-H4ac reveals a slight reduction in H4ac and H2Aac in *H2A-S15A*, and to a lesser extent in *H2A-S15E*, compared to wild type. Histone H3 was used as a loading control. (G) *H2A-S15A/E* show reduced H4ac signal in regions close to the DNA break site. Signal for H4ac was normalized for histone occupancy on total H4 signal. ChIP-qPCR was performed as described for panel D, with primers flanking 150 bp, 1 kb, and 3 kb (left) and 0.5 kb, 1 kb, and 3 kb (right) of DSB.

occurrence of other modifications in chromatin, thus forming a network of histone cross talk (16). H4S1ph carried out by CK2 has been shown to inhibit acetylation of various lysine residues on the N-terminal tail of H4 and play an active role in DSB repair as well as transcription (19, 20). This raised the question of whether H2AS15ph could influence acetylation of lysine residues on the H2A and H4 N-terminal tails. Western blotting analysis of whole-cell extracts from yeast cells grown in normal conditions which harbor *H2A-S15* point mutants reveals a small decrease in both H2A and H4 acetylation, more noticeable in the *H2A-S15A* mutants compared to the wild type (Fig. 1F). We further investigated *in vivo* if the *H2A-S15* mutants affected the acetylation of histones around DSBs. Both *H2A-S15A/E* mutants show a decrease in H4 acetylation signal, but only close to the DNA break site (Fig. 1G). These results suggest that H2AS15ph has a small but significant effect on other histone modifications in regions surrounding the DSB.

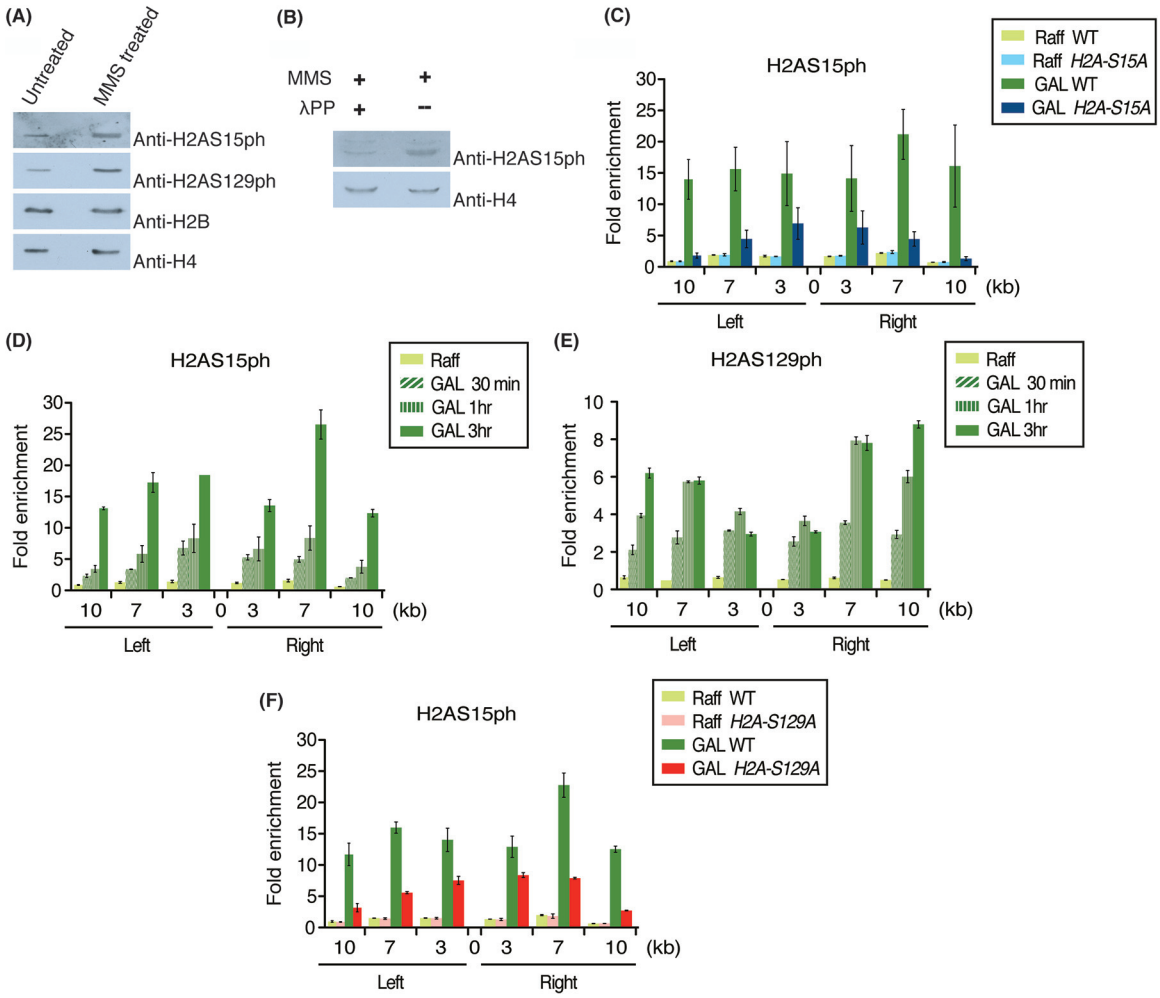

FIG 2 H2AS15ph is locally induced upon DNA double strand break formation and spread over several kilobases. (A) H2AS15ph signal increased when yeast cells were treated with the DNA damaging agent MMS. Western blotting analysis was performed with 300 ng of native chromatin purified from yeast cells treated with DMSO (untreated control) or MMS. Anti-H2AS129ph was used as a positive control for the MMS treatment. Antibodies against histones H2B and H4 were used as loading controls. (B) Anti-H2AS15ph is specific for recognizing a phosphorylation mark on H2A. Western blotting analysis was performed with 300 ng of native chromatin purified from MMS-treated yeast cells after incubation with or without lambda protein phosphatase (λPP). Lane with λPP treatment showed a significant decrease in signal for H2A-S15ph. Histone H4 was used as a loading control. (C) H2AS15ph spreads on both sides of the HO endonuclease-induced single DSB at the *MAT* locus. The signal for H2AS15ph showed enrichment after the induction of the DSB in wild type but not in *H2A-S15A*. ChIP-qPCR was performed as described for Fig. 1D. Fold enrichment was calculated as ratio of percent IP/input normalized on total H4 for histone occupancy at indicated loci around the DSB to the signal at the negative control locus intergenic V. (D, E) Kinetics of H2S15ph and H2AS129ph accumulation after the induction of the HO DSB. ChIP samples were analyzed at 0 min, 30 min, 1 h, and 3 h after HO induction. Anti-H4 signal was used to normalize for histone occupancy. Enrichments were measured as described for panel C. (F) Decreased H2AS15ph signals in cells lacking γ-H2A. ChIP-qPCR of H2AS15ph before and after HO induction in wild type and *H2A-S129A* mutant cells. Enrichments were measured as described for panel C.

H2AS15ph is induced over a large chromatin domain surrounding a DNA double-strand break. To characterize the dynamics of H2AS15ph in response to DNA damage, we produced and purified an antibody against the *S. cerevisiae* H2A N-terminal portion with Ser15 bearing the phosphorylation mark. To demonstrate that H2AS15ph is indeed regulated by DNA damage, we performed immunoblotting with purified yeast native chromatin. As shown in Fig. 2A, the H2AS15ph signal increases with MMS treatment, similarly to H2AS129ph. A control using phosphatase treatment of the chromatin confirms that the signal detected by the antibody is indeed phosphorylation specific (Fig. 2B).

To determine whether H2AS15ph occurs at the DSB, we performed ChIP-qPCR at the *MAT* locus both before and after HO induction. The signal detected for H2AS15ph shows a clear increase around the DSB site in WT background, spanning over 10 kb on each side of the break (Fig. 2C). As a control to check the specificity of the signal detected by the antibody,

the *H2A-S15A* mutant cells do not show such a signal over a large domain after induction of the DSB (Fig. 2C). However, close to the break site, *H2A-S15A* mutant cells do show a slight increase which likely reflects some nonspecific cross-reactivity of the antibody with another mark. To characterize the dynamics of H2AS15ph appearance around the DSB, the ChIP-qPCRs were performed at different time points after induction of the HO endonuclease. Interestingly, the appearance of H2AS15ph seems delayed in comparison to H2AS129ph, reaching maximum levels throughout the region after 3 h, while H2AS129ph reaches its maximum levels at 3 and 7 kb within an hour (Fig. 2D and E). Since H2AS129ph seems to be deposited before H2AS15ph, we tested whether it is required for H2AS15 phosphorylation to occur. ChIP-qPCR in wild type and H2AS129A mutant cells does show a significant decrease in H2AS15ph signal around the HO-induced DSB, but the mark is still present (Fig. 2F). These results indicate that γ-H2A/H2AS129ph can influence phosphorylation of H2AS15 around the DSB but is not required *per se* for it to occur, in agreement with the increased DNA damage sensitivity of the double mutants (Fig. 1B). Altogether, these data clearly demonstrate that H2AS15ph is actively deposited over a large region of chromatin surrounding a DNA double-strand break.

Mec1^{ATR} is solely responsible for H2AS15 phosphorylation at DSBs. Tel1^{ATM}- and Mec1^{ATR}-signaling kinases phosphorylate histone H2AS129 to form γ-H2A (7, 11, 31). They also target various proteins to modulate DSB repair and checkpoint activation. Recruitment of Tel1 to DSB requires Xrs2 (mammalian NBS1), a subunit of the Mre11-Rad50-Xrs2 (MRX) complex (32). Deletion of *XRS2* affects Tel1-dependent checkpoint signaling and telomere maintenance functions (33). Yeast Lcd1/Ddc2 (mammalian ATRIP) is responsible for recruiting Mec1 to RPA-coated single-stranded DNA (ssDNA) produced during end resection (34). Mec1 has been shown to be involved in the spreading of γ-H2A in *trans* onto adjacent undamaged chromosomes in close physical proximity (10, 35). Deletion of *LCD1* leads to the loss of Mec1 recruitment to RPA-coated ssDNA and, therefore, to the loss of Mec1-dependent cell signaling in response to damage (36, 37).

*lcd1*Δ and *lcd1*Δ *xrs2*Δ mutant cells, respectively, are defective in the recruitment of Mec1 and both Mec1 and Tel1 at the DSB. In *lcd1*Δ cells, where Tel1 recruitment and signaling is unaffected, ChIP-qPCR experiments have shown that the signal for γ-H2A close to the break is similar to that of wild type cells (Fig. 3A). However, farther from the break, at 7 kb and 10 kb, the signal is significantly reduced, showing its relation to Mec1. In *lcd1* Δ*xrs2*Δ cells, where both Mec1 and Tel1 recruitments are abrogated, the γ-H2A signal is completely abolished throughout the region (Fig. 3A). This is similar to what has been observed for *mec1*Δ and *mec1*Δ *tel1*Δ mutant cells in previous studies (10). Loss of *MEC1* affects the spreading of γ-H2A away from the break site, whereas loss of *MEC1* and *TEL1* results in the complete loss of γ-H2A.

A large scale phosphoproteomic study has detected phosphorylation of H2AS15 and linked it to Mec1 (29). To investigate this, we carried out ChIP-qPCR using the H2AS15ph antibody to study its spreading around the DSB in *lcd1*Δ and *lcd1*Δ *xrs2*Δ mutant cells. As shown above, wild type cells show enrichment for H2AS15ph over a large region on each side of the DSB (Fig. 3B). However, *lcd1*Δ and *lcd1*Δ *xrs2*Δ mutant cells do not show any H2AS15ph signal. These results demonstrate that, unlike γ-H2A which is deposited by both the Mec1 and Tel1 kinases, H2AS15 phosphorylation is carried out solely by Mec1, which links it to DNA end resection after DSB formation.

H2AS15 is required to maintain fidelity of resection. Previous studies have shown that the *H2A-S129A* nonphosphorylation mutant leads to faster resection from the HO-induced DSB compared to wild type cells (38, 39). This increased resection may be attributed to the inability of Rad9 to bind H2AS129ph through its BRCT domain, an essential interaction for its recruitment on chromatin (17, 27, 28, 40, 41). Budding yeast Rad9, like its mammalian homolog 53BP1, functions in slowing down or checking the rate of DNA end resection (42–45). To investigate whether H2AS15ph may affect resection, we used an antibody against Rfa1, the largest RPA subunit, as a proxy for the ssDNA generated by resection in ChIP-qPCR at the HO-induced DSB. Interestingly, *H2A-S15E* (phosphorylation-mimicking) mutant cells show increased RPA binding near the break, whereas *H2A-S15A* mutant cells behave like wild type cells (Fig. 4A). The *H2A-S129A* cells also show increased RPA signals, reflecting higher ssDNA/resection in this mutant. The double mutants *H2A-S15A/E H2A-S129A* have similar increased

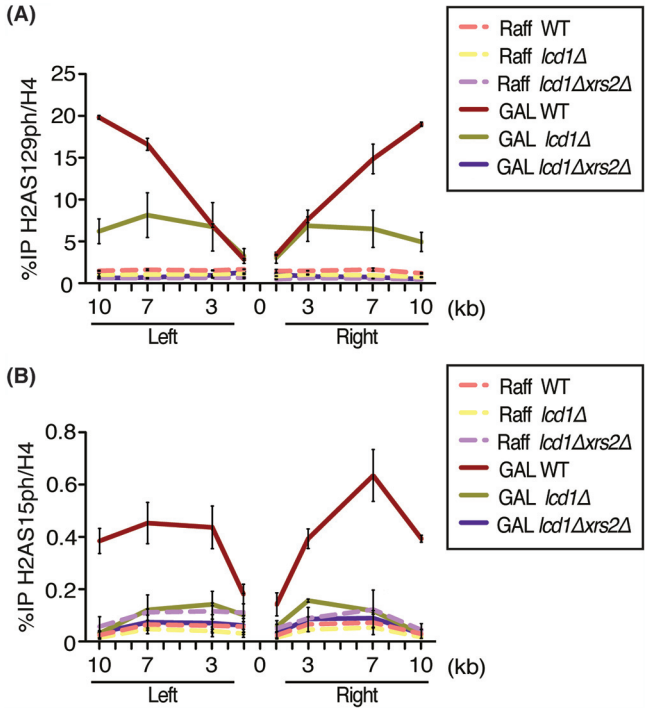

FIG 3 Mec1^{ATR} mediates phosphorylation of H2AS15 *in vivo*. (A) Phosphorylation of H2AS129 carried out by Mec1^{ATR} and Tel1^{ATM}. Signal for H2AS129ph at DSB in *lcd1*Δ (loss of Mec1) is similar to wild type proximal to the break but much reduced distal to the break. H2AS129ph signal is abolished in *lcd1*Δ *xrs2*Δ (loss of Mec1 and Tel1). The line representing the signal for GAL *lcd1*Δ *xrs2*Δ is hidden behind since it has similar values as uninduced/raffinose samples. (B) Phosphorylation of H2AS15 is only mediated by Mec1^{ATR}. Loss of H2AS15ph signal in *lcd1*Δ and *lcd1*Δ *xrs2*Δ compared to WT. All yeast stains used in the above experiments have a *sml1*Δ background. ChIP-qPCR was performed as described for Fig. 1D, primer pairs flanking 1 kb left and right of DSB were also used.

RPA signals to *H2A-S129A* cells, possibly slightly less than *H2A-S15E* cells at some locations (Fig. 4A). To confirm that these RPA signals are the consequence of increased DNA end resection, we used qPCR to directly measure the DNA signal 5 kb away from the DSB, compared to an unrelated genomic locus. In this assay, a significant and similar decrease of signal was detected in *H2A-S15E*, *H2A-S129A*, and double mutants but not in *H2A-S15A* (Fig. 4B). These results indicate that H2AS15 phosphorylation leads to increased resection at DSBs, similar to the effect of losing H2AS129 phosphorylation. Furthermore, the effects of each mutant are nonadditive, suggesting that they are mechanistically related. An interesting possibility is that H2AS15ph is also recognized by the BRCT domain of Rad9, this domain being well characterized for its ability to bind H2AS129ph (27). Surprisingly, *in vitro* peptide-binding assays with recombinant Rad9 indicate a clear binding preference for the histone H2A tail peptide, but in its nonphosphorylated form (Fig. 4B). Importantly, this binding specificity was also confirmed using yeast whole-cell extracts in peptide pulldowns and by detecting endogenous Rad9 using immunoblotting (Fig. 4C). In this case, inducing DNA damage in the cells does not affect endogenous Rad9 ability to bind the H2A peptide *in vitro*. This ability of H2AS15ph to block Rad9 binding to the H2A histone tail may partially explain the increased end resection detected in *H2A-S15E* mutant cells but not in *H2A-S15A* (Fig. 4A and B). As these results suggest that Rad9 directly binds histone H2A tail in chromatin *in vivo*, and that H2AS15 phosphorylation may regulate this interaction, we analyzed Rad9 binding near the HO-induced DSB by ChIP-qPCR. In wild-type conditions in this specific yeast genetic background, we could only detect Rad9-myc signal by ectopic expression from a plasmid. Furthermore, the specific signal based on the empty vector control could only be detected very close (150 bp) on each side of the HO break (Fig. 4E). At these locations, Rad9 binding is abrogated in the *H2A-S129A* mutant, as expected, validating the specificity of the signal. In contrast, Rad9 binding does not seem to be affected by *H2A-S15A/E* mutations.

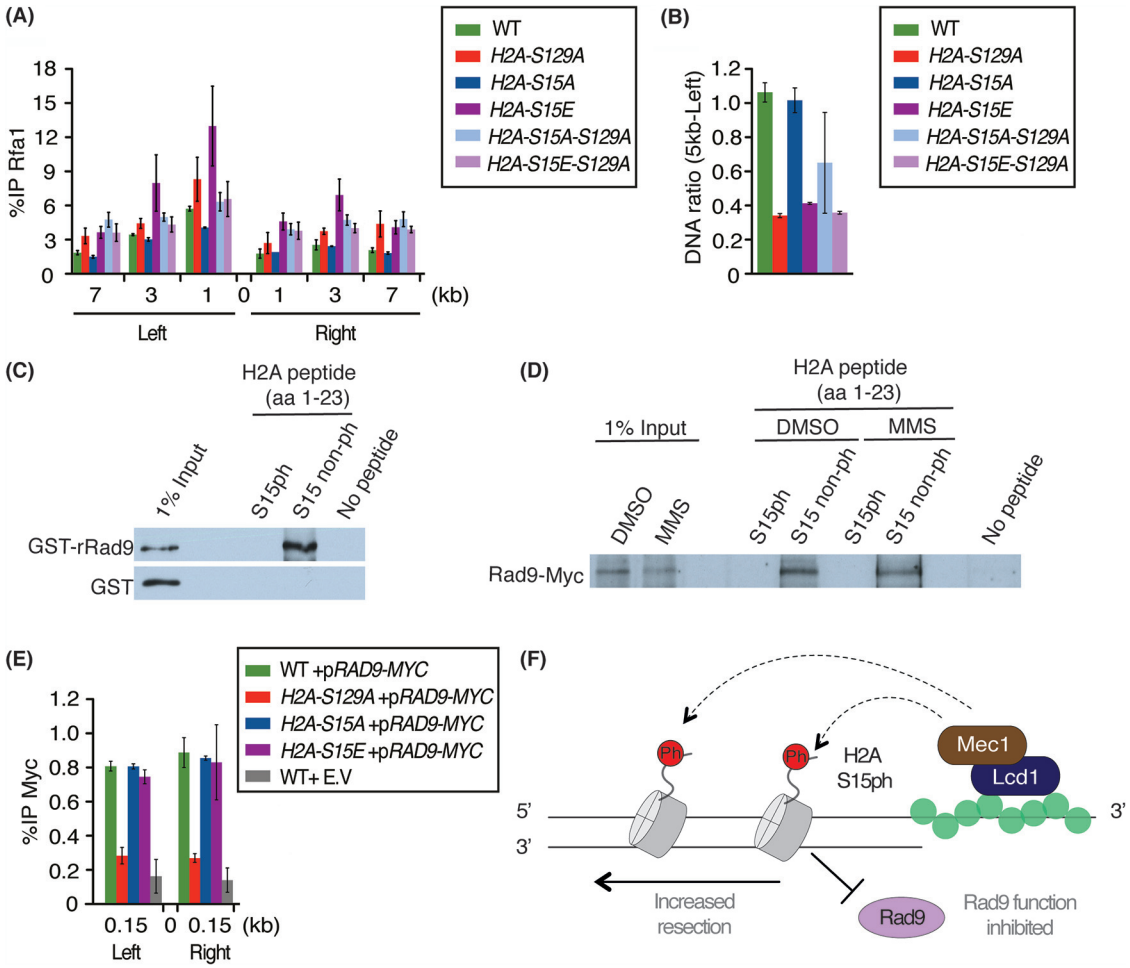

FIG 4 H2AS15 regulates resection of DNA ends at DSB and Rad9^{53BP1} binding *in vitro*. (A) *H2A-S15E* mutant has increased DNA end resection compared to *H2A-S15A* and wild type backgrounds, as shown by single-strand DNA binding RPA signal. *H2A-S129A* is used as a positive control as it also leads to higher resection/RPA binding. ChIP-qPCR was performed as described for Fig. 1D with an antibody against Rfa1 (the largest RPA subunit) and primer pairs flanking 1 kb, 3 kb, and 7 kb to the left and right of DSB. (B) Increased DNA end resection in the *H2A-S15E* mutant is also confirmed by directly measuring DNA signal loss near the HO DSB. After 3 h in inducing media, qPCR was used to measure DNA at 4.8 kb left of the HO cut-site and at control locus in the genome (*PRE1*). Signal ratios on the control locus are decreased in *H2A-S15E* and *H2A-S129A* mutants, indicating similar higher-end resection in these cells. (C) Peptide pulldown assay with GST-tagged recombinant Rad9 and indicated H2A N-terminal peptides. rRad9 binds to unmodified peptide over phosphorylated peptide. Empty GST is used as a negative control. (D) Peptide pulldown assay as in panel B but using extracts from yeast cells treated or not treated with MMS and expressing myc-tagged Rad9. (E) Binding of Rad9 close to the HO DSB is not affected by the H2AS15 mutants *in vivo*. ChIP-qPCRs of Rad9-Myc ectopically expressed in the indicated backgrounds show significant binding within 150 bp of the break, which is lost in the *H2A-S129A* mutant but not in the *H2A-S15E* mutant. A strain with an empty vector (EV) is used as control for background nonspecific Myc signal. (F) Model for the role of H2AS15ph in DSB repair. Mec1 phosphorylates H2AS15 in the region surrounding the DSB. This phosphorylation blocks Rad9 from binding to the H2A tail in the bound nucleosomes, which disrupts its function and results in increased resection. H2AS15ph may function as a dynamic switch to modulate resection, phosphorylation-enabling resection and nonphosphorylation-preventing hyper-resection.

Since H2AS15 phosphorylation occurs further downstream from the DNA break, the Rad9 signal detected here, close to the HO site, may not reflect the population regulated by H2AS15ph (see references 42 and 46 for models of two populations/functions of Rad9/53BP1 near DNA ends versus larger domains). Another possibility is that H2AS15ph is not required for Rad9 recruitment but regulates the way it binds nucleosomes and influences end resection. Altogether, these results implicate the DNA damage-induced H2AS15ph histone mark in the regulation of end resection at DSBs.

DISCUSSION

Histone tails are sites of various posttranslational modifications (PTMs) such as phosphorylation, acetylation, methylation, ubiquitylation, and SUMOylation. These modifications are

recognized by reader proteins containing specialized domains such as ubiquitin binding domains, BRCT and FHA domains which bind phosphorylation, chromodomains, MBT domains, bromodomains, and PHD fingers that recognize methylation or acetylation. Proteins and protein complexes use these interactions for their proper recruitment, retention, and/or orientation at the target sites to carry out their respective functions (47, 48).

In this study, we characterized yeast H2AS15ph as a novel histone modification in the context of DNA damage. This modification is induced in the presence of DNA damaging agent MMS, which is a known alkylating agent and produces DSBs as cells replicate their DNA in S-phase. A large-scale proteomic study had identified H2AS15ph by mass spectrometry and implicated Mec1^{ATR} for its detection (29). Using *in vivo* analysis, we show that indeed Mec1, and not Tel1, is responsible for the induction of this mark around DNA breaks, unlike γ-H2A (H2AS129ph) which is deposited by either Tel1 or Mec1 (Fig. 3). While the spreading of γ-H2A at DSBs is not affected in *H2A-S15A/E* mutant cells, the *H2A-S129A* mutant does affect the levels of H2AS15ph (Fig. 1C to D; Fig. 2F). Furthermore, a decrease in chromatin acetylation was detected in *H2A-S15A/E* mutant cells near the DNA break (Fig. 1F and G). We know from previous studies that the acetylation of histones H4 and H2A by the NuA4 complex plays an important role in the recruitment of various chromatin remodelers, such as INO80, RSC, and SWI/SNF, required for repair by HR (12, 49–51). Future work will be needed to determine if H2AS15 affects the recruitment of these remodelers.

A most interesting finding reported here is that yeast H2AS15ph corresponds to an evolutionary conserved function to regulate 53BP1/Rad9 binding to the H2A tail and DNA end resection. The yeast H2AS15 residue seems to be the functional homolog of mammalian H2AK15 in modulating resection, which in turn affects DNA repair pathway selection, albeit through different PTMs. In mammals, when 53BP1 binds H2AK15ub in the vicinity of DSBs, it inhibits resection and favors the NHEJ pathway. This binding inhibits TIP60-mediated acetylation of H4 and H2A tails in chromatin, including H2AK15, which otherwise would block ubiquitylation by RNF168 and 53BP1 binding, favoring resection and HR (25). *H2A-S15E* mutant cells show increased resection, as seen with *H2A-S129A* mutant cells where Rad9^{53BP1} is incapable of binding and inhibiting or slowing down resection (Fig. 4A and B). *In vitro* data suggest that Rad9 binds the H2A N-terminal tail in its unmodified state and that this binding is abolished when H2AS15 is phosphorylated (Fig. 4C to D). On the other hand, this regulated interaction does not seem to affect Rad9 recruitment to the DSB (Fig. 4E). Since Rad9 is recruited to nucleosomes near DSBs though bivalent interaction with H2AS129ph and H3K79me, our results suggest that Rad9 interaction with the H2A tail is not required for its recruitment but can regulate its function linked to DNA end resection. 53BP1 also interacts with nucleosomes through three interfaces: H2AK15ub-UDR, H4K20me-Tudor, and H2A.XS139ph-BRCT. But, as in yeast, only two are required for its binding to nucleosomes, γ-H2AX–BRCT being dispensable (24, 46, 52). We proposed a model (depicted in Fig. 4F) where resection of DNA ends produces ssDNA, which becomes coated by RPA and recruits Mec1^{ATR} through its binding partner Lcd1/Ddc2^{ATRIP} (34, 36). Mec1 then phosphorylates H2AS15, inhibiting Rad9 function and therefore increasing resection. H2AS15ph may be a dynamic mark, switching between phosphorylation and nonphosphorylation states to fine-tune the process of resection. This conserved function of the H2A tail to regulate Rad9/53BP1 binding and resection is supported even further by a recent report showing phosphorylation of the ubiquitin moiety of H2AK15ub (H2AK15pUbT12) inhibits 53BP1 binding and favors resection (53).

Future work will address whether specific proteins may bind H2AS15ph. While our peptide pulldowns with yeast extracts, followed by mass spectrometry, did not yield clear results (data not shown), we speculate that other DNA repair proteins, such as Rtt107 and Dpb11 which have BRCT domains, could recognize H2AS15ph. Rtt107 was recently shown to bind H4T80ph and γ-H2A to counteract Rad9-modulated checkpoint activity (54). Dpb11 has been shown to act as a scaffold protein for various checkpoint proteins and it is involved in Rad9 recruitment/retention at DSBs (55, 56). H2AS15 may also act redundantly with other DNA damage-induced histone phosphorylation marks and function as a scaffold for proper orientation or retention of repair factors.

MATERIALS AND METHODS

Yeast strains. All yeast strains used in the current study are from FY406 (57) and JKM179 (58) (*hta1-htb1*Δ::*NatMX*, *hta2-htb2*Δ::*KANMX*) backgrounds, with deletion of both copies of H2A and H2B genes. These strains carry an ectopic copy of *HTA1-HTB1* on low-copy-number vector pRS413 (in FY406) or pRS414 (in JKM179). Gene deletion and point mutations were obtained through standard PCR techniques. Plasmid shuffling using 5-fluoroorotic acid was used to introduce the plasmid with point mutations in each respective background. Yeast background JKM139 (58) with deletion of *sml1*Δ::*NATMX*, *lcd1*Δ::*KANMX*, *xrs2*Δ::*TRP1* was used in this study. QY362 (JKM139 *RAD9-13MYC*::*KANMX*) was used for peptide pulldown experiments, while the Rad9-Myc ChIP-qPCR were done in the JKM179 background with *HTA1/2-HTB1/2* deletions covering wild type or mutant H2A and ectopic Rad9-Myc expression from a pRS315 vector (40). General lithium acetate method was used to transform the yeast cells. Cells were grown in yeast extract-peptone-dextrose (YPD; 1% yeast extract, 2% peptone, 2% dextrose) at 30°C until the early log phase. For the spot assay, a 1:10 dilution of the culture was spotted and grown at 30°C for 3 to 4 days.

Chromatin Immunoprecipitation (ChIP). ChIP-qPCR was performed as described previously (59). In brief, cells were grown overnight in YP-raffinose until reaching an OD_{600} of 0.5 to 1, at which point galactose (2%) was added to induce DSB at the *MAT* locus for 3 h. This was followed by cross-linking of cells with formaldehyde and lysing via bead beating. Sonication was performed with a Diagenode Bioruptor to obtain a chromatin size of ~200 to 500 bp. One hundred μg of chromatin was used to set up the immunoprecipitation reaction with anti-H2A-S129ph (upstate 07-745), anti-H2A-S15ph (antibody was produced in rabbit using the peptide sequence Ac-GSAAKA(pS)QSRSAK-C. Affinity purification was performed to improve the specificity of the antibody, with phosphorylated versus nonphosphorylated peptides. Antibody was produced by Thermo Fisher Scientific), anti-Rfa1 (Agrisera AS07214), anti-H4ac (Upstate 06-946), anti-H4 (Abcam 7311), and anti-Myc (9E10 Babco MMS150R), and the reaction was allowed to mix on a wheel overnight at 4°C. The next morning, protein A-agarose beads (Protein-G Magnetic beads for anti-Myc) were added, followed by an additional 3 to 4 h on a wheel at 4°C. After multiple washing steps, the DNA was eluted and incubated at 65°C overnight for de-cross-linking followed by phenol-chloroform extraction of DNA. This DNA was resuspended in NTE and used for qPCR. An LC480 LightCycler (Roche) was used to quantify DNA with the primer pairs, as indicated in the corresponding figures, to calculate the percentage of the immunoprecipitation (IP)/input. The data represent the mean of two independent biological replicates. Error bars indicate the ranges between the two biological replicates. Fold enrichment represents ratio of percent IP/input at indicated loci around DSB normalized on signal at negative-control locus intergenic V. The levels of HO-induced DNA break were verified by qPCR across the HO cut site (normalized on control locus) and were similar in all experiments. Direct measurement of end resection by qPCR was done using primers 4.8 kb left of the HO cut site and presented as a ratio of signal over a control locus (*PRE1* [60]). Primer sequences are available upon request.

Purification of native yeast chromatin. Native yeast chromatin was prepared as described previously (61), and cells were treated with MMS (0.05%) or dimethyl sulfoxide (DMSO; control) for 2 h to induce DNA damage. Lambda protein phosphatase (λPP; NEB) was used to dephosphorylate the purified chromatin. The reaction mixture was incubated for 30 min at 30°C, followed by a booster of λPP and incubation for an additional 30 min at 30°C.

Recombinant protein purification. Recombinant Rad9 (C-terminal containing Tudor and BRCT domains) protein was purified as described previously (62). In short, bacterial cells were grown overnight at 16°C with isopropyl-β-D-thiogalactopyranoside induction. The next day, cells were lysed with lysozyme followed by sonication. The soluble portion was incubated with glutathione-Sepharose beads (GE Healthcare) for 3 to 4 h at 4°C and eluted with glutathione. The eluted protein concentration was quantified by running on SDS-PAGE with known BSA standards, followed by Coomassie staining.

Peptide pulldown. Peptide pulldown was performed with synthetic peptide corresponding to H2A N-terminal (aa 1 to 23) obtained from AnaSpec. One microgram of peptide was incubated with 1 μg of glutathione *S*-transferase (GST)-tagged protein overnight on a wheel at 4°C in binding buffer (50 mM Tris-HCl [pH 7.5], 50 mM NaCl, 0.1% NP-40, 1 mM phenylmethylsulfonyl fluoride [PMSF] and phosphatase inhibitors). The next morning, streptavidin Dynabeads were added to the reaction mixture and kept at 4°C for an additional 2 hours, followed by washing, running on SDS-PAGE, and Western blotting with anti-GST (Sigma G1160).

Peptide pulldowns with yeast cell extracts were performed by growing cells in YPD and treating with MMS (0.05%) or DMSO for 2 h (final OD_{600} ~ 1.0 to 1.5). Cells were centrifuged, and the pellet was washed with cold Milli-Q water, resuspended in sensitization buffer (100 mM Tris-HCl [pH 9.4], 10 mM dithiothreitol [DTT]), and incubated at 30°C on a wheel for 15 min. It was then centrifuged at 500 $\times$ *g* for 5 mins at 4°C, resuspended in 30 ml of spheroplasting buffer (1.2 M sorbitol, 20 mM HEPES [pH 7.5]), centrifuged again, resuspended in 40 ml of spheroplasting buffer with lyticase, and incubated on a wheel at 30°C for 90 min. After centrifugation at 500 $\times$ *g* for 5 min and washing with wash buffer [1.2 M sorbitol, 20 mM piperazine-*N*,*N*′-bis(2-ethanesulfonic acid) (PIPES; pH 6.4), 1 mM $MgCl_2$), it was resuspended in 25 ml of nuclear isolation buffer (NIB; 250 mM sucrose, 60 mM KCl, 1 mM PMSF, 14 mM NaCl, 0.8% Triton X-100, 5 mM $MgCl_2$, 1 mM $CaCl_2$, 15 mM morpholineethanesulfonic acid), mixed well to remove clumps, and kept on ice for 20 min. After centrifugation and two washes with NIB (until white nuclear pellet was obtained), the pellet was resuspended in pulldown buffer (400 mM NaCl, 1 mM PMSF, 50 mM Tris-HCl [pH 8], 0.5% NP-40, 5 mM β-glycerophosphate, 10 mM sodium butyrate, 5 mM NaF) to get 300 mM NaCl in the final volume, followed by incubation on a rotating plate at 4°C for 20 min. After centrifugation at 14,000 rpm at 4°C for 30 min, the supernatant was collected (nuclear extract). Biotinylated peptides were bound to streptavidin Dynabeads in peptide-binding buffer (150 mM NaCl, 50 mM Tris-HCl [pH 8.0], 0.1% NP-40, 5 mM β-glycerophosphate, 10 mM sodium butyrate, 5 mM NaF) by incubating at room temperature on a wheel for 30 min. Peptide-Dynabeads were washed with protein-binding buffer (140 mM NaCl, 50 mM Tris-HCl [pH 8.0], 0.1% NP-40, 0.5 mM DTT, 10 μM $ZnCl_2$, 5 mM β-glycerophosphate, 10 mM sodium butyrate, 5 mM NaF) followed by the

addition of 600 μg of nuclear extract to each pulldown reaction and were then incubated at 4°C on a wheel for 2 h. Nuclear extract that was incubated with phospho peptide was initially incubated with nonphospho peptide; while nuclear extract for nonphospho peptide was initially incubated with phospho peptide for 2 h at 4°C on a wheel. After three to four washes with final wash buffer (350 mM NaCl, 50 mM Tris-HCl [pH 8.0], 0.1% NP-40, 0.5 mM DTT, 10 μM $ZnCl_2$, 5 mM β-glycerophosphate, 10 mM sodium butyrate, 5 mM NaF), Laemmli buffer was added, boiled, and resolved in SDS-PAGE, followed by Western blotting with anti-Myc (9E10 Babco MMS150R).

ACKNOWLEDGMENTS

We thank Xue Cheng for important advice. We are grateful to Jim Haber for sharing reagents/strains and stimulating discussions.

This work was supported by a grant from the Canadian Institutes of Health Research (CIHR) to J.C. (FDN-143314). S.A. held a Desjardins/Fondation du CHU de Québec studentship. J.C. holds the Canada Research Chair in Chromatin Biology and Molecular Epigenetics.

REFERENCES

1. Hanahan D, Weinberg RA. 2011. Hallmarks of cancer: the next generation. Cell 144:646–674. https://doi.org/10.1016/j.cell.2011.02.013.
2. Jackson SP, Bartek J. 2009. The DNA-damage response in human biology and disease. Nature 461:1071–1078. https://doi.org/10.1038/nature08467.
3. Chiruvella KK, Liang Z, Wilson TE. 2013. Repair of double-strand breaks by end joining. Cold Spring Harb Perspect Biol 5:a012757. https://doi.org/10.1101/cshperspect.a012757.
4. Symington LS. 2016. Mechanism and regulation of DNA end resection in eukaryotes. Crit Rev Biochem Mol Biol 51:195–212. https://doi.org/10.3109/10409238.2016.1172552.
5. Abraham RT. 2001. Cell cycle checkpoint signaling through the ATM and ATR kinases. Genes Dev 15:2177–2196. https://doi.org/10.1101/gad.914401.
6. Smith GC, Jackson SP. 1999. The DNA-dependent protein kinase. Genes Dev 13:916–934. https://doi.org/10.1101/gad.13.8.916.
7. Downs JA, Lowndes NF, Jackson SP. 2000. A role for *Saccharomyces cerevisiae* histone H2A in DNA repair. Nature 408:1001–1004. https://doi.org/10.1038/35050000.
8. Paull TT, Rogakou EP, Yamazaki V, Kirchgessner CU, Gellert M, Bonner WM. 2000. A critical role for histone H2AX in recruitment of repair factors to nuclear foci after DNA damage. Curr Biol 10:886–895. https://doi.org/10.1016/s0960-9822(00)00610-2.
9. Rogakou EP, Boon C, Redon C, Bonner WM. 1999. Megabase chromatin domains involved in DNA double-strand breaks *in vivo*. J Cell Biol 146:905–916. https://doi.org/10.1083/jcb.146.5.905.
10. Lee CS, Lee K, Legube G, Haber JE. 2014. Dynamics of yeast histone H2A and H2B phosphorylation in response to a double-strand break. Nat Struct Mol Biol 21:103–109. https://doi.org/10.1038/nsmb.2737.
11. Shroff R, Arbel-Eden A, Pilch D, Ira G, Bonner WM, Petrini JH, Haber JE, Lichten M. 2004. Distribution and dynamics of chromatin modification induced by a defined DNA double-strand break. Curr Biol 14:1703–1711. https://doi.org/10.1016/j.cub.2004.09.047.
12. Downs JA, Allard S, Jobin-Robitaille O, Javaheri A, Auger A, Bouchard N, Kron SJ, Jackson SP, Côté J. 2004. Binding of chromatin-modifying activities to phosphorylated histone H2A at DNA damage sites. Mol Cell 16:979–990. https://doi.org/10.1016/j.molcel.2004.12.003.
13. Morrison AJ, Highland J, Krogan NJ, Arbel-Eden A, Greenblatt JF, Haber JE, Shen X. 2004. INO80 and gamma-H2AX interaction links ATP-dependent chromatin remodeling to DNA damage repair. Cell 119:767–775. https://doi.org/10.1016/j.cell.2004.11.037.
14. van Attikum H, Fritsch O, Gasser SM. 2007. Distinct roles for SWR1 and INO80 chromatin remodeling complexes at chromosomal double-strand breaks. EMBO J 26:4113–4125. https://doi.org/10.1038/sj.emboj.7601835.
15. van Attikum H, Fritsch O, Hohn B, Gasser SM. 2004. Recruitment of the INO80 complex by H2A phosphorylation links ATP-dependent chromatin remodeling with DNA double-strand break repair. Cell 119:777–788. https://doi.org/10.1016/j.cell.2004.11.033.
16. Dantuma NP, van Attikum H. 2016. Spatiotemporal regulation of post-translational modifications in the DNA damage response. EMBO J 35:6–23. https://doi.org/10.15252/embj.201592595.
17. Wysocki R, Javaheri A, Allard S, Sha F, Côté J, Kron SJ. 2005. Role of Dot1-dependent histone H3 methylation in G_1 and S phase DNA damage checkpoint functions of Rad9. Mol Cell Biol 25:8430–8443. https://doi.org/10.1128/MCB.25.19.8430-8443.2005.
18. Celeste A, Petersen S, Romanienko PJ, Fernandez-Capetillo O, Chen HT, Sedelnikova OA, Reina-San-Martin B, Coppola V, Meffre E, Difilippantonio MJ, Redon C, Pilch DR, Olaru A, Eckhaus M, Camerini-Otero RD, Tessarollo L, Livak F, Manova K, Bonner WM, Nussenzweig MC, Nussenzweig A. 2002. Genomic instability in mice lacking histone H2AX. Science 296:922–927. https://doi.org/10.1126/science.1069398.
19. Cheung WL, Turner FB, Krishnamoorthy T, Wolner B, Ahn SH, Foley M, Dorsey JA, Peterson CL, Berger SL, Allis CD. 2005. Phosphorylation of histone H4 serine 1 during DNA damage requires casein kinase II in *S. cerevisiae*. Curr Biol 15:656–660. https://doi.org/10.1016/j.cub.2005.02.049.
20. Utley RT, Lacoste N, Jobin-Robitaille O, Allard S, Cote J. 2005. Regulation of NuA4 histone acetyltransferase activity in transcription and DNA repair by phosphorylation of histone H4. Mol Cell Biol 25:8179–8190. https://doi.org/10.1128/MCB.25.18.8179-8190.2005.
21. Harvey AC, Jackson SP, Downs JA. 2005. *Saccharomyces cerevisiae* histone H2A Ser122 facilitates DNA repair. Genetics 170:543–553. https://doi.org/10.1534/genetics.104.038570.
22. Krishnamoorthy T, Chen X, Govin J, Cheung WL, Dorsey J, Schindler K, Winter E, Allis CD, Guacci V, Khochbin S, Fuller MT, Berger SL. 2006. Phosphorylation of histone H4 Ser1 regulates sporulation in yeast and is conserved in fly and mouse spermatogenesis. Genes Dev 20:2580–2592. https://doi.org/10.1101/gad.1457006.
23. House NCM, Polleys EJ, Quasem I, De la Rosa Mejia M, Joyce CE, Takacsi-Nagy O, Krebs JE, Fuchs SM, Freudenreich CH. 2019. Distinct roles for *S. cerevisiae* H2A copies in recombination and repeat stability, with a role for H2A.1 threonine 126. Elife 8:e53362. https://doi.org/10.7554/eLife.53362.
24. Fradet-Turcotte A, Canny MD, Escribano-Díaz C, Orthwein A, Leung CC, Huang H, Landry MC, Kitevski-LeBlanc J, Noordermeer SM, Sicheri F, Durocher D. 2013. 53BP1 is a reader of the DNA-damage-induced H2A Lys 15 ubiquitin mark. Nature 499:50–54. https://doi.org/10.1038/nature12318.
25. Jacquet K, Fradet-Turcotte A, Avvakumov N, Lambert JP, Roques C, Pandita RK, Paquet E, Herst P, Gingras AC, Pandita TK, Legube G, Doyon Y, Durocher D, Côté J. 2016. The TIP60 complex regulates bivalent chromatin recognition by 53BP1 through direct H4K20me binding and H2AK15 acetylation. Mol Cell 62:409–421. https://doi.org/10.1016/j.molcel.2016.03.031.
26. Grenon M, Costelloe T, Jimeno S, O'Shaughnessy A, FitzGerald J, Zgheib O, Degerth L, Lowndes NF. 2007. Docking onto chromatin via the *Saccharomyces cerevisiae* Rad9 Tudor domain. Yeast 24:105–119. https://doi.org/10.1002/yea.1441.
27. Hammet A, Magill C, Heierhorst J, Jackson SP. 2007. Rad9 BRCT domain interaction with phosphorylated H2AX regulates the G1 checkpoint in budding yeast. EMBO Rep 8:851–857. https://doi.org/10.1038/sj.embor.7401036.
28. Javaheri A, Wysocki R, Jobin-Robitaille O, Altaf M, Cote J, Kron SJ. 2006. Yeast G1 DNA damage checkpoint regulation by H2A phosphorylation is independent of chromatin remodeling. Proc Natl Acad Sci U S A 103:13771–13776. https://doi.org/10.1073/pnas.0511192103.
29. Bastos de Oliveira FM, Kim D, Cussiol JR, Das J, Jeong MC, Doerfler L, Schmidt KH, Yu H, Smolka MB. 2015. Phosphoproteomics reveals distinct modes of Mec1/ATR signaling during DNA replication. Mol Cell 57:1124–1132. https://doi.org/10.1016/j.molcel.2015.01.043.
30. Allard S, Utley RT, Savard J, Clarke A, Grant P, Brandl CJ, Pillus L, Workman JL, Côté J. 1999. NuA4, an essential transcription adaptor/histone H4 acetyltransferase complex containing Esa1p and the ATM-related

cofactor Tra1p. EMBO J 18:5108–5119. https://doi.org/10.1093/emboj/18.18.5108.
31. Redon C, Pilch DR, Rogakou EP, Orr AH, Lowndes NF, Bonner WM. 2003. Yeast histone 2A serine 129 is essential for the efficient repair of checkpoint-blind DNA damage. EMBO Rep 4:678–684. https://doi.org/10.1038/sj.embor.embor871.
32. Nakada D, Matsumoto K, Sugimoto K. 2003. ATM-related Tel1 associates with double-strand breaks through an Xrs2-dependent mechanism. Genes Dev 17:1957–1962. https://doi.org/10.1101/gad.1099003.
33. Oh J, Al-Zain A, Cannavo E, Cejka P, Symington LS. 2016. Xrs2-Dependent and Independent Functions of the Mre11-Rad50 Complex. Mol Cell 64:405–415. https://doi.org/10.1016/j.molcel.2016.09.011.
34. Zou L, Elledge SJ. 2003. Sensing DNA damage through ATRIP recognition of RPA-ssDNA complexes. Science 300:1542–1548. https://doi.org/10.1126/science.1083430.
35. Li K, Bronk G, Kondev J, Haber JE. 2020. Yeast ATM and ATR kinases use different mechanisms to spread histone H2A phosphorylation around a DNA double-strand break. Proc Natl Acad Sci U S A 117:21354–21363. https://doi.org/10.1073/pnas.2002126117.
36. Gobbini E, Cesena D, Galbiati A, Lockhart A, Longhese MP. 2013. Interplays between ATM/Tel1 and ATR/Mec1 in sensing and signaling DNA double-strand breaks. DNA Repair (Amst)) 12:791–799. https://doi.org/10.1016/j.dnarep.2013.07.009.
37. Paciotti V, Clerici M, Lucchini G, Longhese MP. 2000. The checkpoint protein Ddc2, functionally related to S. pombe Rad26, interacts with Mec1 and is regulated by Mec1-dependent phosphorylation in budding yeast. Gen Dev 14:2046–2059.
38. Chen X, Cui D, Papusha A, Zhang X, Chu CD, Tang J, Chen K, Pan X, Ira G. 2012. The Fun30 nucleosome remodeller promotes resection of DNA double-strand break ends. Nature 489:576–580. https://doi.org/10.1038/nature11355.
39. Eapen VV, Sugawara N, Tsabar M, Wu WH, Haber JE. 2012. The *Saccharomyces cerevisiae* chromatin remodeler Fun30 regulates DNA end resection and checkpoint deactivation. Mol Cell Biol 32:4727–4740. https://doi.org/10.1128/MCB.00566-12.
40. Nnakwe CC, Altaf M, Cote J, Kron SJ. 2009. Dissection of Rad9 BRCT domain function in the mitotic checkpoint response to telomere uncapping. DNA Repair (Amst)) 8:1452–1461. https://doi.org/10.1016/j.dnarep.2009.09.010.
41. Toh GW, O'Shaughnessy AM, Jimeno S, Dobbie IM, Grenon M, Maffini S, O'Rorke A, Lowndes NF. 2006. Histone H2A phosphorylation and H3 methylation are required for a novel Rad9 DSB repair function following checkpoint activation. DNA Repair (Amst)) 5:693–703. https://doi.org/10.1016/j.dnarep.2006.03.005.
42. Ferrari M, Dibitetto D, De Gregorio G, Eapen VV, Rawal CC, Lazzaro F, Tsabar M, Marini F, Haber JE, Pellicioli A. 2015. Functional interplay between the 53BP1-ortholog Rad9 and the Mre11 complex regulates resection, end-tethering and repair of a double-strand break. PLoS Genet 11:e1004928. https://doi.org/10.1371/journal.pgen.1004928.
43. Escribano-Díaz C, Orthwein A, Fradet-Turcotte A, Xing M, Young JT, Tkáč J, Cook MA, Rosebrock AP, Munro M, Canny MD, Xu D, Durocher D. 2013. A cell cycle-dependent regulatory circuit composed of 53BP1-RIF1 and BRCA1-CtIP controls DNA repair pathway choice. Mol Cell 49:872–883. https://doi.org/10.1016/j.molcel.2013.01.001.
44. Noordermeer SM, Adam S, Setiaputra D, Barazas M, Pettitt SJ, Ling AK, Olivieri M, Alvarez-Quilon A, Moatti N, Zimmermann M, Annunziato S, Krastev DB, Song F, Brandsma I, Frankum J, Brough R, Sherker A, Landry S, Szilard RK, Munro MM, McEwan A, Goullet de Rugy T, Lin ZY, Hart T, Moffat J, Gingras AC, Martin A, van Attikum H, Jonkers J, Lord CJ, Rottenberg S, Durocher D. 2018. The shieldin complex mediates 53BP1-dependent DNA repair. Nature 560:117–121. https://doi.org/10.1038/s41586-018-0340-7.
45. Zimmermann M, Lottersberger F, Buonomo SB, Sfeir A, de Lange T. 2013. 53BP1 regulates DSB repair using Rif1 to control 5′ end resection. Science 339:700–704. https://doi.org/10.1126/science.1231573.
46. Bothmer A, Robbiani DF, Di Virgilio M, Bunting SF, Klein IA, Feldhahn N, Barlow J, Chen HT, Bosque D, Callen E, Nussenzweig A, Nussenzweig MC. 2011. Regulation of DNA end joining, resection, and immunoglobulin class switch recombination by 53BP1. Mol Cell 42:319–329. https://doi.org/10.1016/j.molcel.2011.03.019.
47. Wilson MD, Durocher D. 2017. Reading chromatin signatures after DNA double-strand breaks. Philos Trans R Soc Lond B Biol Sci 372. https://doi.org/10.1098/rstb.2016.0280.
48. Rossetto D, Truman AW, Kron SJ, Cote J. 2010. Epigenetic modifications in double-strand break DNA damage signaling and repair. Clin Cancer Res 16:4543–4552. https://doi.org/10.1158/1078-0432.CCR-10-0513.
49. Bennett G, Peterson CL. 2015. SWI/SNF recruitment to a DNA double-strand break by the NuA4 and Gcn5 histone acetyltransferases. DNA Repair (Amst) 30:38–45. https://doi.org/10.1016/j.dnarep.2015.03.006.
50. House NCM, Yang JH, Walsh SC, Moy JM, Freudenreich CH. 2014. NuA4 initiates dynamic histone H4 acetylation to promote high-fidelity sister chromatid recombination at postreplication gaps. Mol Cell 55:818–828. https://doi.org/10.1016/j.molcel.2014.07.007.
51. Cheng X, Cote V, Cote J. 2021. NuA4 and SAGA acetyltransferase complexes cooperate for repair of DNA breaks by homologous recombination. PLoS Genet 17:e1009459. https://doi.org/10.1371/journal.pgen.1009459.
52. Zgheib O, Pataky K, Brugger J, Halazonetis TD. 2009. An oligomerized 53BP1 Tudor domain suffices for recognition of DNA double-strand breaks. Mol Cell Biol 29:1050–1058. https://doi.org/10.1128/MCB.01011-08.
53. Walser F, Mulder MPC, Bragantini B, Burger S, Gubser T, Gatti M, Botuyan MV, Villa A, Altmeyer M, Neri D, Ovaa H, Mer G, Penengo L. 2020. Ubiquitin phosphorylation at Thr12 modulates the DNA damage response. Mol Cell 80:423–436.e9. https://doi.org/10.1016/j.molcel.2020.09.017.
54. Millan-Zambrano G, Santos-Rosa H, Puddu F, Robson SC, Jackson SP, Kouzarides T. 2018. Phosphorylation of histone H4T80 triggers DNA damage checkpoint recovery. Mol Cell 72:625–635.e4. https://doi.org/10.1016/j.molcel.2018.09.023.
55. Liu Y, Cussiol JR, Dibitetto D, Sims JR, Twayana S, Weiss RS, Freire R, Marini F, Pellicioli A, Smolka MB. 2017. TOPBP1(Dpb11) plays a conserved role in homologous recombination DNA repair through the coordinated recruitment of 53BP1(Rad9). J Cell Biol 216:623–639. https://doi.org/10.1083/jcb.201607031.
56. Granata M, Lazzaro F, Novarina D, Panigada D, Puddu F, Abreu CM, Kumar R, Grenon M, Lowndes NF, Plevani P, Muzi-Falconi M. 2010. Dynamics of Rad9 chromatin binding and checkpoint function are mediated by its dimerization and are cell cycle-regulated by CDK1 activity. PLoS Genet 6:e1001047. https://doi.org/10.1371/journal.pgen.1001047.
57. Hirschhorn JN, Bortvin AL, Ricupero-Hovasse SL, Winston F. 1995. A new class of histone H2A mutations in *Saccharomyces cerevisiae* causes specific transcriptional defects in vivo. Mol Cell Biol 15:1999–2009. https://doi.org/10.1128/MCB.15.4.1999.
58. Lee SE, Moore JK, Holmes A, Umezu K, Kolodner RD, Haber JE. 1998. *Saccharomyces* Ku70, Mre11/Rad50, and RPA proteins regulate adaptation to G2/M arrest after DNA damage. Cell 94:399–409. https://doi.org/10.1016/s0092-8674(00)81482-8.
59. Rossetto D, Cramet M, Wang AY, Steunou AL, Lacoste N, Schulze JM, Cote V, Monnet-Saksouk J, Piquet S, Nourani A, Kobor MS, Cote J. 2014. Eaf5/7/3 form a functionally independent NuA4 submodule linked to RNA polymerase II-coupled nucleosome recycling. EMBO J 33:1397–1415. https://doi.org/10.15252/embj.201386433.
60. Mojumdar A, Sorenson K, Hohl M, Toulouze M, Lees-Miller SP, Dubrana K, Petrini JHJ, Cobb JA. 2019. Nej1 interacts with Mre11 to regulate tethering and Dna2 Binding at DNA double-strand breaks. Cell Rep 28:1564–1573.e3. https://doi.org/10.1016/j.celrep.2019.07.018.
61. Altaf M, Utley RT, Lacoste N, Tan S, Briggs SD, Cote J. 2007. Interplay of chromatin modifiers on a short basic patch of histone H4 tail defines the boundary of telomeric heterochromatin. Mol Cell 28:1002–1014. https://doi.org/10.1016/j.molcel.2007.12.002.
62. Setiaputra D, Ahmad S, Dalwadi U, Steunou A-L, Lu S, Ross JD, Dong M-Q, Côté J, Yip CK. 2018. Molecular architecture of the essential yeast histone acetyltransferase complex NuA4 redefines its multimodularity. Mol Cell Biol 38:e00570-17. https://doi.org/10.1128/MCB.00570-17.